



The cell-permeable iron chelator M606 inhibits MYCN-driven neuroblastoma via an E2F3-mediated response

Ruby Pandher^{a,1}, Chengyuan Xue^{a,1} , Laura D. Gamble^a , Giorgio Milazzo^b , Simone Di Giacomo^b , Jayne Murray^a, Leanna Cheung^a , Francesca Ferrucci^b, Marta Palombo^b, Stefania Purgato^b, Catherine A. Burkhardt^c , Natalia Fedtsova^d, Anatoli S. Gleiberman^e , Andrei A. Purmal^e, Lioubov Korotchkina^e, Mikhail A. Nikiforov^d, Sergei S. Makarov^f , Thomas J. Telfer^g , Rachel Codd^g , Glenn M. Marshall^{a,h} , David A. Scottⁱ , Andrei L. Ostermanⁱ , Andrei V. Gudkov^d , Giovanni Perini^{b,j,2} , Michelle Haber^{a,2} , and Murray D. Norris^{a,k,2,3}

Affiliations are included on p. 11.

Edited by Robert Eisenman, Fred Hutchinson Cancer Research Center, Seattle, WA; received October 2, 2024; accepted April 16, 2025

Despite Myc oncoproteins being major causal factors in human cancer, they remain “undruggable.” The *MYCN* oncogene is one of the most powerful prognostic markers for the childhood cancer neuroblastoma and represents an important target for developing novel therapeutics. Here, we report the finding and characterization of M606, a selective small molecule inhibitor of MYCN, which was identified by screening a diverse chemical library. M606 reduced MYCN protein levels in neuroblastoma cell lines and upregulated hypoxia-inducible factor 1 alpha (HIF1A). Using siRNA-mediated knockdown of *MYCN*, *c-Myc*, or *HIF1A* in HepG2 and BE(2)-C cells followed by M606 treatment, we demonstrated that Myc downregulation and HIF1A upregulation were two independent effects of M606 treatment. M606 selectively targeted neuroblastoma cell lines expressing higher levels of MYCN protein and delayed neuroblastoma development in the *TH-MYCN* transgenic mouse model. Metabolomic analysis showed that M606 modulated glucose metabolism, consistent with a hypoxic response and iron deprivation. Biochemical characterization of M606 not only confirmed its iron-chelating properties but also revealed its ability to downregulate *MYCN* promoter activity, which could be rescued by the addition of iron. Luciferase assays identified the minimal *MYCN* promoter region required for the M606 response, which contained overlapping E2F transcription factor binding sites. Further evaluation defined a key role for E2F3 in the M606-mediated response. The finding of a potent cell-permeable iron chelator that can chelate iron to directly downregulate *MYCN* transcription via an E2F3-mediated response represents a potentially valuable therapeutic approach in the treatment of cancers overexpressing Myc oncoproteins.

iron chelation | *MYCN* oncogene | neuroblastoma | E2F

Neuroblastoma is the most prevalent solid tumor in early childhood, with a median age at diagnosis of 18 mo (1, 2). The tumors arise from the developing sympathetic nervous system (1, 2). Despite intensive treatment regimens involving high-dose chemotherapy with stem-cell support, radiotherapy, and immunotherapy, event-free survival rates remain poor at around 50% for high-risk neuroblastoma, with surviving patients suffering significant life-long morbidities from the significant immediate and late toxicities from the dose intensification of conventional chemotherapy and radiotherapy (3–6). Moreover, high-risk neuroblastoma is frequently resistant to standard of care therapies and prone to relapse, at which point children have very few treatment options.

The most malignant neuroblastomas harbor amplification of the *MYCN* oncogene, found in approximately 20 to 30% of patients (7, 8). *MYCN* amplification is associated with aggressive disease and poor outcome (7, 8). MYCN is a part of the Myc family of oncoproteins, including *c-Myc*, and *MycL*, all of which share significant homology in protein sequence and function. As a family of basic helix–loop–helix leucine zipper transcription factors, Myc proteins regulate the expression of up to 15% of all genes in the human genome (9). These proteins form heterodimers with the basic helix–loop–helix molecule, Max, and bind to DNA through canonical and noncanonical E-box sequences (CACGTG/CANNTG) to drive transcription of target genes that are important for proliferation, differentiation, metabolism, and apoptosis. Under normal conditions, Myc expression is tightly regulated. However, Myc deregulation is a major causal factor in many human cancers and can occur due to insertional mutagenesis, chromosomal translocation, and gene amplification (9). The frequent deregulation of Myc and the high dependency of tumor growth on elevated Myc levels suggest that this oncoprotein represents a valuable target for cancer therapy (10–12).

Significance

Neuroblastoma is the most common solid tumor diagnosed in infants, and amplification of the *MYCN* oncogene occurs in 40 to 50% of high-risk neuroblastomas, serving as a powerful marker of aggressive disease and poor overall outcome. We identified and characterized M606, an iron-chelating small-molecule MYCN/*c-Myc* inhibitor. We demonstrated that *MYCN*-amplified neuroblastomas are sensitive to M606 via an E2F3-mediated response at the *MYCN* promoter. Our study highlights the clinical potential of reducing MYCN expression using a cell-permeable iron chelator as a therapeutic strategy against *MYCN*-amplified neuroblastoma.

Author contributions: A.V.G., G.P., M.H., and M.D.N. designed research; R.P., C.X., L.D.G., G.M., S.D.G., J.M., L.C., F.F., M.P., S.P., C.A.B., N.F., A.S.G., A.A.P., L.K., M.A.N., S.S.M., T.J.T., R.C., and D.A.S. performed research; A.L.O., A.V.G., G.P., M.H., and M.D.N. contributed new reagents/analytic tools; R.P., G.M., J.M., A.S.G., A.P.P., S.S.M., T.J.T., R.C., G.M.M., D.A.S., A.L.O., A.V.G., G.P., M.H., and M.D.N. analyzed data; and R.P., M.H., and M.D.N. wrote the paper.

The authors declare no competing interest.

This article is a PNAS Direct Submission.

Copyright © 2025 the Author(s). Published by PNAS. This open access article is distributed under Creative Commons Attribution-NonCommercial-NoDerivatives License 4.0 (CC BY-NC-ND).

¹R.P. and C.X. contributed equally to this work.

²G.P., M.H., and M.D.N. contributed equally to this work.

³To whom correspondence may be addressed. Email: MNorris@ccia.unsw.edu.au.

This article contains supporting information online at <https://www.pnas.org/lookup/suppl/doi:10.1073/pnas.2420011122/-DCSupplemental>.

Published June 2, 2025.

In contrast to Myc oncoproteins, the retinoblastoma tumor suppressor (RB) functions as a master cell cycle regulator and frequently displays a loss of function in cancer cells. This loss of function through mutation or functional inactivation results in RB dissociation from E2F transcription factors, activation of the S phase of the cell cycle, and increased cell proliferation (13, 14). E2F proteins also regulate *MYCN* transcription and are essential for maintaining *MYCN* activity in neuroblastoma cells (15, 16). These findings suggest that members of the E2F family may be valuable therapeutic targets in *MYCN*-amplified neuroblastoma.

Despite its clear role in neuroblastoma pathogenesis, *MYCN* has remained undruggable, while the need for novel therapeutic strategies that are more targeted and less toxic remains high. Highly proliferative *MYCN*-driven neuroblastoma cells have a dependency on iron that exceeds that of normal cells, and iron chelation therapy offers a potential novel therapeutic approach in this disease (17), although to date clinical trials have largely proved disappointing (18). Here, we performed screening of a diverse small molecule chemical library using a cell-based readout system and identified M606 as a potent cell-permeable iron chelator that reduces *MYCN* protein expression by acting on the *MYCN* promoter via E2F3-mediated transcription factor binding sites.

Results

Chemical Library Screening Identified M606 as a MYC/N Inhibitor. To identify small molecule inhibitors of *MYCN*, we developed a cell-based readout system using the SHR6-17 cell line (SHEP neuroblastoma cells containing a *MYC*-responsive luciferase reporter) that can respond to exogenously introduced *MYCN* (19). A chemical library of 34,000 diverse molecules was screened for compounds that inhibited *MYC*-responsive promoter activity following the transduction of cells with *MYCN* lentivirus. After filtering out false positives (19), 12 putative *MYCN* inhibitors were identified, representing multiple structural classes. The compounds fell into two categories: one group (N423F7, N269D8, N77A7, N103A8, and N147A7) affected *MYCN*

transcriptional activity by downregulating *MYCN* protein and the second group (e.g., N4G6) inhibited *MYC/N* transcriptional activity without altering *MYCN* protein levels (Fig. 1A and *SI Appendix*, Fig. S1A). The putative *MYC/N* inhibitors reversed the expression of both positively (*thymidylate synthase*)- and negatively (*p27/kip1*)-regulated *MYC/N* target genes similarly to *MYC* shRNA (*SI Appendix*, Fig. S1A).

To identify more potent compounds, focused libraries were designed around the N269D8 quinoline class of compounds (Fig. 1B) because this molecule had the greatest effect on both *MYCN* protein expression and the transactivation of endogenous targets. Related quinoline derivatives were identified that had similar activity to N269D8. Further evaluation of this class of compounds was undertaken with M606 (Fig. 1B) due to its availability and stability. In addition to abrogating *MYCN* transactivation (*SI Appendix*, Fig. S1B), M606 reduced *MYCN* mRNA levels in the *MYCN*-amplified human neuroblastoma cell line BE(2)-C in a time-dependent manner (*SI Appendix*, Fig. S1C). Furthermore, M606 reduced *MYCN* protein levels in BE(2)-C cells and c-MYC protein levels in the human hepatoblastoma cell line, HepG2, in a dose- (Fig. 1C) and time-dependent manner (Fig. 1D).

M606 Inhibits Cell Proliferation and Exhibits Anticancer Effects In Vitro and In Vivo. To assess the effect of M606 on cell proliferation, EdU incorporation assays were performed in SHR6-17 cells, the cell line used in the original screen. A dose-dependent reduction in EdU incorporation was observed following treatment with M606, with more pronounced effects observed after 48 h (Fig. 2A). Similar effects were observed in vivo, with reduced EdU incorporation observed in the colons of NIH Swiss mice treated with a single dose of M606 at 10 mg/kg, compared to DMSO-treated mice (Fig. 2B).

Given the reduction in cell proliferation observed, we performed clonogenic assays on *MYCN*-amplified BE(2)-C and LAN-1 neuroblastoma cells treated with 1 to 5 μ M M606. Both cell lines exhibited a dose-dependent reduction in clonogenic

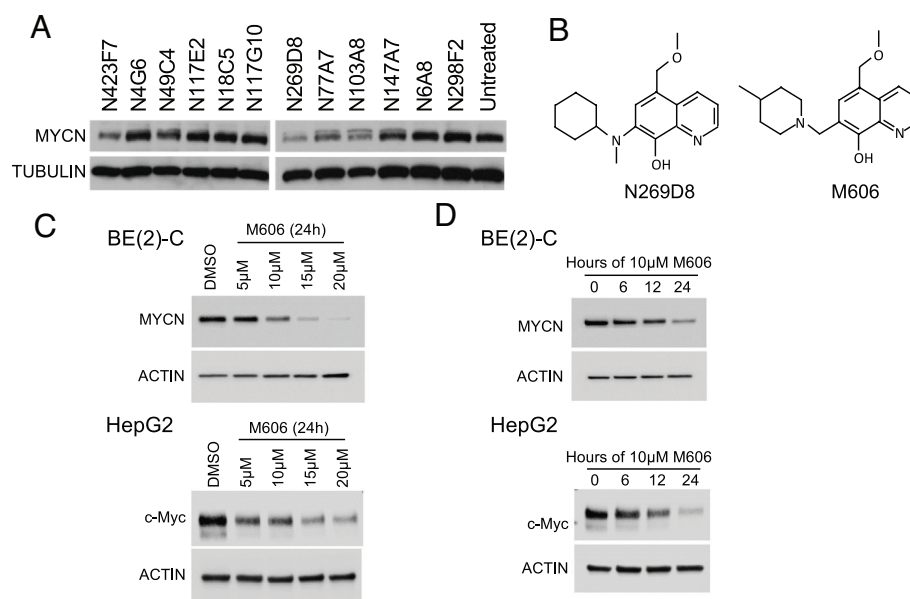


Fig. 1. Chemical library screening identifies M606 as a Myc/N inhibitor. (A) Following the exclusion of false positives, 12 compounds that reduced *MYC* transcription/luciferase activity in *MYCN*-transduced SHEP cells were tested for their ability to reduce *MYCN* protein in IMR-32 cells after treatment with 10 μ M for 48 h. (B) Focused libraries were generated around confirmed hits for secondary screening. Attention was paid to the N269D8 quinoline class, which had the greatest effects on *MYCN* expression and transactivation of endogenous targets. M606, a structurally related quinoline derivative, was identified and investigated further. Western blot analysis of c-Myc and *MYCN* in BE(2)-C and HepG2 cells following M606 treatment at various concentrations (C) and for different lengths of time (D).

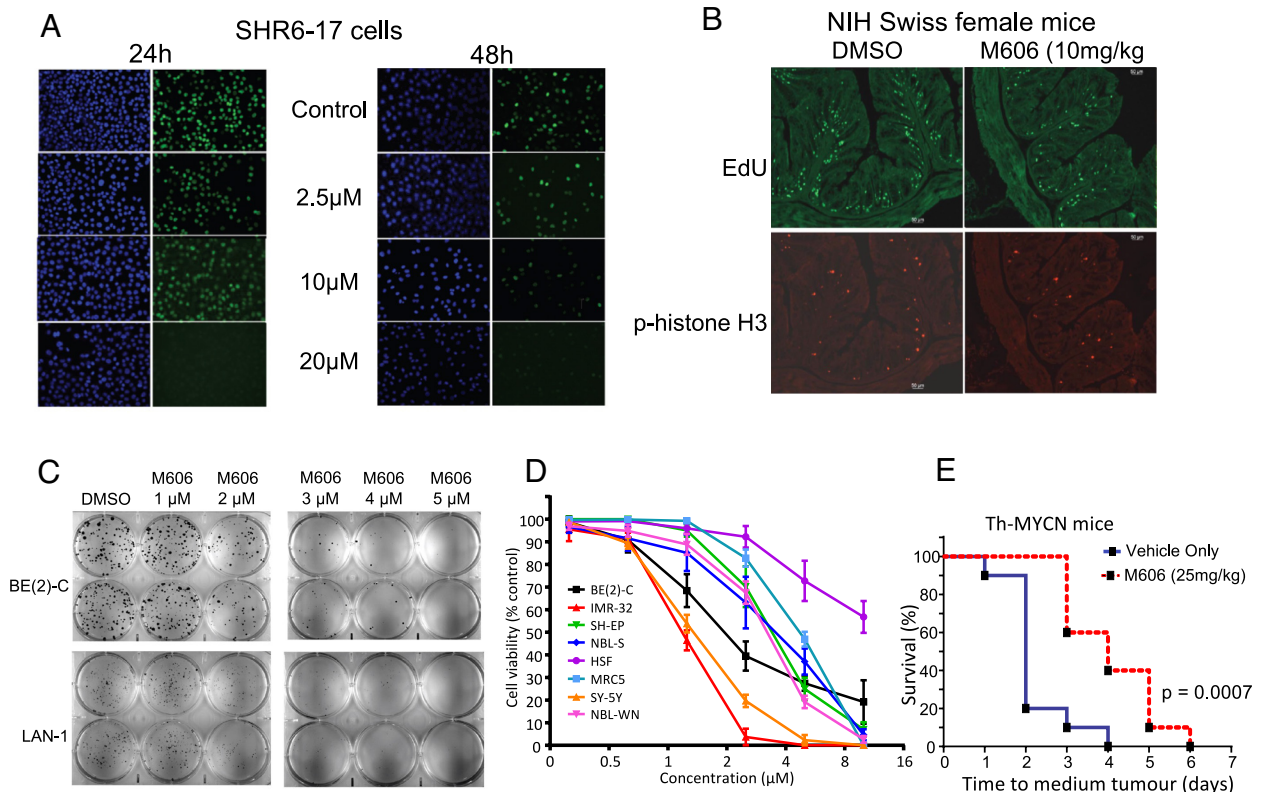


Fig. 2. Effects of M606 on MYC-expressing cell lines and tumor formation in *TH-MYC* mice. (A) SHR6-17 cells were exposed to different concentrations of M606 for 24 h and 48 h, and the level of EdU incorporated (green) into the DNA of these cells was measured by fluorescent microscopy. DAPI stained nuclei are shown in blue. (B) Female NIH Swiss mice (18-wk-old) were treated with a single injection of M606 (10 mg/kg). Phospho-histone H3 was used as a mitosis marker (red). (C) Colony formation assays were performed using BE(2)-C and LAN-1 neuroblastoma cells. Cells were treated with escalating doses of M606 for 72 h and then allowed to form colonies for 14 d. (D) MYCN-expressing neuroblastoma cell lines and normal diploid fibroblasts were cultured in medium supplemented with increasing doses of M606 for 72 h. Viability was measured using the Alamar Blue viability assay. Data are presented as the mean cell viability \pm SD for three independent biological replicates. (E) Kaplan–Meier survival curves showing the survival of *TH-MYC*^{+/+} transgenic mice after treatment with 25 mg/kg M606 daily once 5-mm tumors were palpable. The log-rank test was used to compare the survival between the control and treated groups using GraphPad software ($*P < 0.05$; $**P < 0.01$; $***P < 0.001$; $****P < 0.0001$).

capacity in the presence of M606 (Fig. 2C). Furthermore, M606 was cytotoxic in a panel of MYCN expressing (BE(2)-C, KELLY, IMR-32, LAN-1, NBL-WN) and c-MYC expressing (NBL-S, SY-5Y, SH-EP) neuroblastoma cell lines, but less cytotoxic to the nonmalignant fibroblast cell lines MRC5 and HSF, suggesting a dependence of neuroblastoma cells on MYC oncoproteins for survival (Fig. 2D). We also evaluated the effects of M606 (25 mg/kg) in the *TH-MYC* transgenic mouse model of neuroblastoma (20) following the development of a small palpable tumor. M606 significantly extended overall survival ($P = 0.0007$) compared to the vehicle control (Fig. 2E). These findings highlight the therapeutic potential of inhibiting MYC as an anticancer treatment.

M606 Induces Transcriptional Activation of MYC-Driven Target Genes. We next sought to determine the specificity of M606 for MYC-mediated transcription compared to other known transcription factors. The Attagene cis-Factorial assay allows the simultaneous evaluation of an agent against 50 distinct transcription factors. Strikingly, M606 demonstrated highly specific effects following a 48 h treatment of HepG2 cells; only two transcription factors were transactivated—MYC and the hypoxia-inducible factor HIF1A (Fig. 3A). Moreover, not only did M606 cause a dose-dependent decrease in MYC-mediated transcription in HepG2 cells but also a dramatic dose-dependent increase in HIF1A (Fig. 3B). The effects of M606 on the other 48 transcription factors tested in the assay were markedly less pronounced.

To verify the functionality of the HIF1A induction by M606, the effects of M606 on the HIF1A target genes *vascular endothelial growth factor (VEGF-A)* and *erythropoietin (EPO)* were determined in HepG2 cells. M606 significantly increased *VEGF-A* expression at both 6 h (~3.5-fold) and 24 h (~11-fold) (Fig. 3C). This level of induction was similar to that caused by the positive control, deferrioxamine (DFO), a clinically used iron chelator and prolyl hydroxylase (PHD) inhibitor (21) known to induce HIF1A. A similar trend was observed for *EPO* expression; however, the changes did not reach statistical significance except for DFO at 6 h (Fig. 3C).

The Effects of M606 on Myc and HIF1A Protein Levels Are Independent Events. Consistent with the effects of M606 on the transcriptional activity of HIF1A, M606 dramatically increased HIF1A protein expression in BE(2)-C and HepG2 cells in a dose- and time-dependent manner (Fig. 3D), with levels comparable to DFO and another PHD inhibitor, dimethylxylglycine (DMOG). The induction of HIF1A occurred much more rapidly than the reduction in MYC/N protein levels suggesting that the effect of M606 on these two proteins may be independent events or that HIF1A may play a role in M606-mediated degradation of MYC proteins (22). To investigate these effects further, HIF1A was depleted in BE(2)-C and HepG2 cells 24 h before M606 treatment to eliminate HIF1A-mediated effects. Under these conditions, M606 still caused a reduction in MYC/N levels in these two cell lines to a level similar to cells treated with control

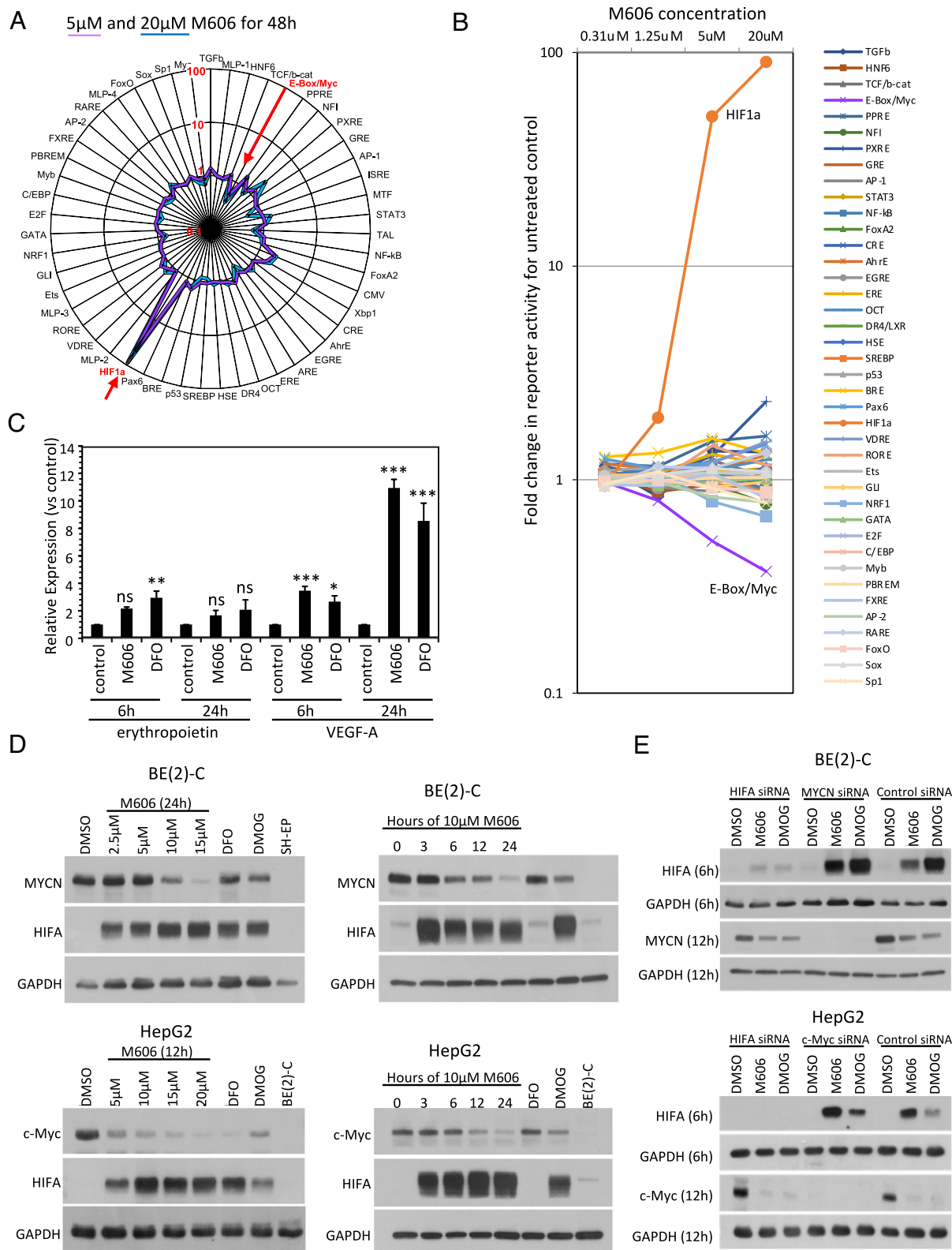


Fig. 3. Specificity of M606 for MYC-mediated transcription compared to other known transcription factors. (A) The Attagene cis-Factorial assay results following treatment of HepG2 cells with 5 µM (purple) or 20 µM (blue) M606 for 48 h. (B) Fold-change in reporter activity following treatment of HepG2 cells with increasing concentrations of M606 compared to untreated cells. (C) Expression of HIF1A target genes by qPCR after treatment with 10 µM of M606 or 100 µM DFO. (**P* < 0.05; ***P* < 0.01; ****P* < 0.001) (D) Western blot analysis of c-MYC, MYCN, and HIF1A in BE(2)-C (Top) and HepG2 cells (Bottom) following treatment with M606 at different concentrations (Left Panel) or for different lengths of time (Right Panel). DFO (100 µM) and DMOG (1 mM) were used as positive controls for HIF1A induction. (E) Western blot analysis for c-Myc, MYCN, and HIF1A following siRNA knockdown of HIF1A or MYCN in BE(2)-C (Top) and HepG2 (Bottom) cells.

siRNA, indicating that HIF1A is not involved in M606-mediated downregulation of the MYC proteins (Fig. 3E). Conversely, MYCN and c-Myc knockdown in the same cell systems did not

prevent M606-mediated HIF1A upregulation (Fig. 3E). Together, these findings demonstrate that the effects of M606 on HIF1A and MYCN or c-Myc are independent events.

M606 Modulates Glucose Metabolism and Inhibits TCA Cycle Activity in Neuroblastoma Cells. Since the stabilization of HIF is known to activate glycolysis, we examined the effects of M606 on glucose metabolism by measuring cellular glucose uptake and lactate secretion. Glycolysis is activated upon stabilization of HIF via the upregulation of major glycolytic enzymes, lactate dehydrogenase, and pyruvate kinase (PKM2) and the suppression of pyruvate dehydrogenase (PDH) activity via activation of PDH kinase (PDK1), which constrains the flow of carbon from glucose to the tricarboxylic acid cycle (TCA). In combination, these effects promote the conversion of pyruvate to lactate and its excretion (23, 24). The analysis of the major glucose metabolites in BE(2)-C cells treated with M606 revealed a ≥ 2 -fold increase in glucose consumption and ≥ 1.5 -fold increase in lactate secretion (but no change in glutamine uptake), which is consistent with HIF stabilization (Fig. 4A). Notably, this effect of M606 treatment was completely reversed with the addition of iron (Fe) in excess levels to M606. Quantification by GC-MS of cellular polar metabolites following treatment with M606 showed a general 2 to 3 \times accumulation of most metabolites in neuroblastoma cells, possibly indicative of growth arrest or blockages in metabolic pathways (SI Appendix, Fig. S2A). Most notably, though, M606 effected much larger increases in lactate (7.5 \times), citrate (50 \times), and succinate (11 \times ; Fig. 4B). While the effect on lactate could be caused by M606-mediated HIF stabilization, the accumulation of the TCA intermediates citrate and succinate may be explained

by the possible inhibition of iron-sulfur (Fe-S) cluster-dependent enzymes, aconitase (ACON), and succinate dehydrogenase, acting downstream of citrate and succinate, respectively. Again, these M606 effects were completely reversed by the addition of iron (Fig. 4B). Dysfunction in the TCA cycle distal to citrate with M606 treatment was also indicated by ^{13}C labeling studies done in parallel with metabolite quantification. The ^{13}C labeling of metabolites in cells labeled with either ^{13}C -glucose or ^{13}C -glutamine was used to calculate the metabolic origin of alpha-ketoglutarate (aKG). In control cells, $\sim 60\%$ of aKG derived from ^{13}C -glutamine, and $\sim 40\%$ from ^{13}C -glucose (via citrate) (SI Appendix, Fig. S2B). With M606 treatment, the input from glutamine was unaffected, but the input from citrate was reduced to $\sim 25\%$, indicating inhibition of the TCA cycle between citrate and aKG (the total inputs to aKG with M606 are $\ll 100\%$, which implies that labeling of aKG does not reach saturation within the 24 h labeling period due to inhibition of citrate to aKG conversion). This inhibition of aKG labeling by M606 was reversed by the addition of iron (SI Appendix, Fig. S2B).

M606 Is an Iron-Chelating Compound. To further explore the link between iron and M606, the mass spectrometric profiles obtained by direct injection of either M606, or M606 plus iron, revealed that three M606 molecules can bind with a single iron (Fe^{3+}) ion as shown by signals at m/z values of 954.4, 477.8, and 318.9, ascribed to single, double, or triple protonated adducts of $\text{Fe}[\text{M606}(1-)]_3$,

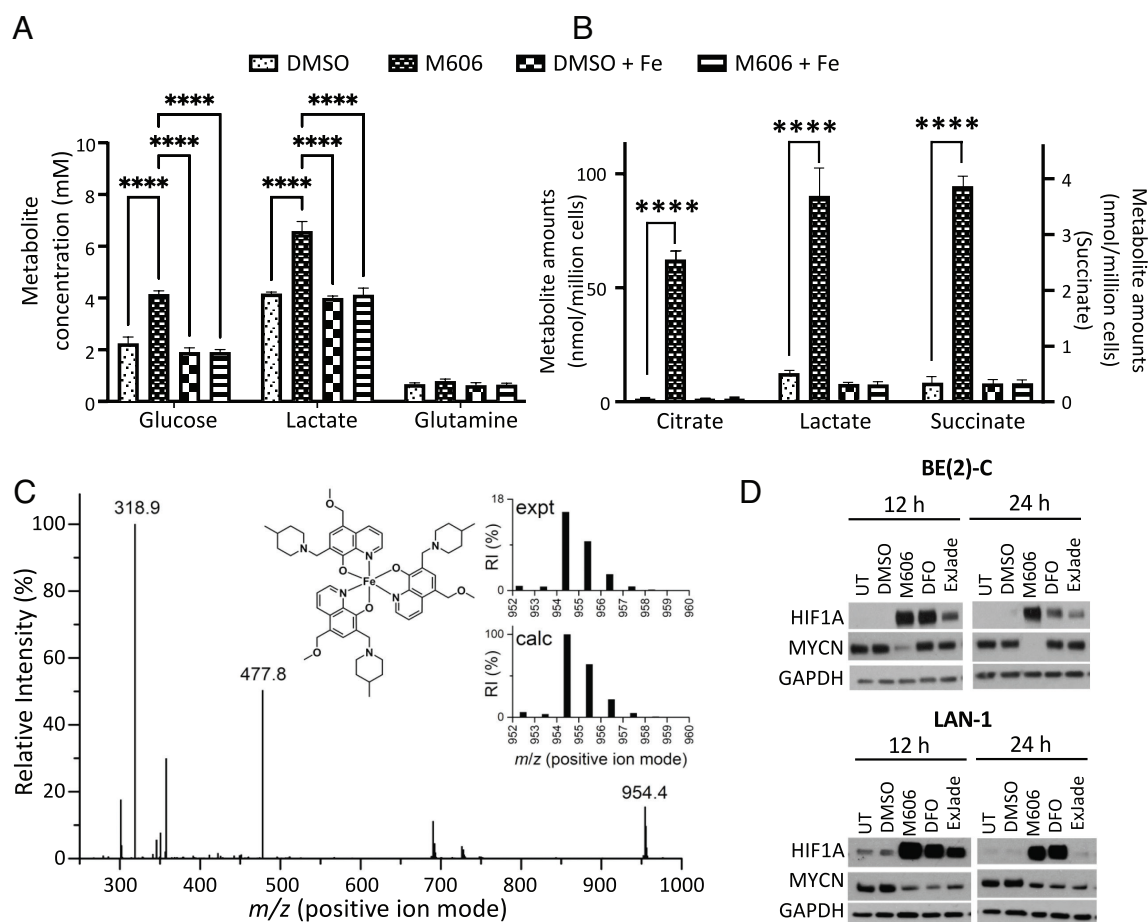


Fig. 4. M606 is an iron chelator that modulates glucose metabolism (A) Determination of extracellular glucose, lactate, glutamate, and glutamine concentration changes by a YSI analyzer in cultures of BE(2)-C cells treated with 5 μM M606, excess iron (III) citrate, or their combination. (B) GC-MS metabolic profiling of intracellular citrate, lactate, and succinate. (**** $p < 0.0001$) (C) Mass spectrum (positive ion mode) from a 1:3 solution of Fe(III):M606 with signals marked as characteristic of the single, double, and triple protonated adducts of the depicted species [M]. The inset shows the experimental (Upper) and calculated (Lower) isotope patterns for the $[M + H]^+$ adduct. (D) Western blot analysis of MYCN and HIF1A in BE(2)-C and LAN-1 cells after treatment with 15 μM M606, DFO, or Exjade for 12 h or 24 h.

respectively (Fig. 4C). Having confirmed the iron-chelating ability of M606, we next compared this compound with current clinically used iron chelators, DFO and Exjade. Cytotoxicity assays were performed in BE(2)-C and LAN-1 neuroblastoma cells following treatment with M606, DFO, and Exjade with or without excess Fe^{3+} added to the culture medium. LAN-1 cells were chosen as a second cell line since DFO had previously been shown to reduce MYCN protein levels in this cell line (25). As shown in *SI Appendix, Fig. S3A*, the addition of iron rescued the cells from each of the three iron chelators, although to a lesser extent for M606. M606 potently reduced MYCN protein levels in both cell lines, while DFO and Exjade had a similar effect in LAN-1 cells, but very little change in BE(2)-C cells (Fig. 4D). The addition of iron reversed the effects of M606 on MYCN protein levels and the induction of HIF1A after 12 h treatment (*SI Appendix, Fig. S3B*). Furthermore, treatment of BE(2)-C cells with M606, DFO, or Exjade for 24 h resulted in the accumulation of cells in the G1 phase of the cell cycle, with a reduction in cells in the S and G2/M phases, while LAN-1 cells demonstrated a less pronounced G1 and G2 arrest (*SI Appendix, Fig. S4*). Importantly, these cell cycle effects could be reversed by the addition of excess iron to both cell lines.

To determine the mechanism by which M606 downregulates MYCN, we investigated the effects of this small molecule on MYCN mRNA and protein stability and found no difference between control and M606-treated BE(2)-C cells (*SI Appendix, Fig. S5A and B*). However, using a luciferase reporter assay, we observed that M606 potently reduced MYCN promoter activity to a greater extent than either DFO or Exjade (*SI Appendix, Fig. S5C*). Measurement of the intracellular accumulation of M606, DFO, and Exjade by liquid chromatography coupled to mass spectrometry (LC-MS) showed that M606 accumulated in both BE(2)-C and LAN-1 cells at much higher levels than Exjade, while DFO was undetectable (*SI Appendix, Fig. S5D*), indicating that the reduction in MYCN promoter activity could be directly correlated with the amount of iron chelator that enters the cells. In addition, we also investigated overexpression of exogenous MYCN without its cognate promoter in SHR6-17 neuroblastoma cells to determine its effect on M606 activity. Lentiviral transduction of SHR6-17 cells with increasing volumes of a pTZV3-N-myc construct yielded SHR6-15.6, SHR6-31.3, SHR6-62.5, and SHR6-250 clones which exhibited increased levels of exogenous MYCN expression. M606 cytotoxicity assays showed that the SHR-62.5 and SHR6-250 cells were up to 2-fold more resistant than the SHR6-0 mock transduced control cells (*SI Appendix, Fig. S5E*) providing further evidence for M606 exerting its effects via the endogenous MYCN promoter.

To directly test whether M606-mediated downregulation of MYC was related to its iron chelating abilities, we generated structural analogs of M606 that could not chelate iron and found these analogs were unable to downregulate MYCN or induce HIF1A (*SI Appendix, Fig. S6*). Furthermore, these analogs abrogated the cytotoxic effects of M606 (*SI Appendix, Fig. S6*). These data suggested that, unlike DFO and to a lesser extent Exjade, M606 could accumulate and remain in cells to exert its effects on the MYCN promoter.

A Region Within the MYCN Promoter Encompassing E2F Binding Sites Determines Sensitivity of Neuroblastoma Cells to M606.

We next sought to identify the minimum response region in the MYCN promoter responsible for the M606-mediated downregulation of MYCN protein levels. Nine different promoter deletions with overlapping regions were cloned into the pGL3-Basic vector (Fig. 5A) and transfected into BE(2)-C cells. The

transfected cells were treated with M606, and promoter activity assays demonstrated that the deletion of Region 8 and, to a lesser degree, Region 9 resulted in a loss of the MYCN promoter response, indicating these regions were the most sensitive to M606 (Fig. 5B and *SI Appendix, Fig. S7A*). To investigate this phenomenon further, constructs of Region 8 and the negative control Region 2 (Fig. 5C and *SI Appendix, Fig. S7B*) were transfected into BE(2)-C and LAN-1 neuroblastoma cells and tested for M606 sensitivity. Only the reintroduction of region 8 restored M606 sensitivity in both cell lines (Fig. 5D and *SI Appendix, Fig. S7C and D*). Region 8 was further divided into three subregions of approximately 100 bp in length (Regions A, B, and C) with a 50-bp overlap (Fig. 5C and *SI Appendix, Fig. S7E*) and transfected into BE(2)-C cells. Only Region 8C remained responsive to M606 (Fig. 5E), indicating this region directly mediated the effects of M606. Sequence analysis of Region 8C found three E2F transcription factor binding consensus sequences and one TGF β inhibitory element (TIE), confirming previous studies that demonstrated that these sites were critical for the activation of the MYCN promoter by E2F1-3 proteins (16).

To further assess the involvement of the E2F sites in mediating the effects of M606, we generated two constructs of the whole MYCN promoter carrying a deletion of 12 bp, corresponding to the E2F sites. The first construct comprised a deletion of two inversely orientated and overlapped E2F sites and the second a deletion of the third E2F and TIE sites. These constructs were transfected into BE(2)-C and LAN-1 cells, and the effects of M606 on reporter activity were assessed. Only the deletion of the E2F-1 and E2F-2 sites resulted in the loss of M606 responsiveness (Fig. 5F and *SI Appendix, Fig. S7F*), suggesting that these binding sites are critical for M606 activity. Similar results were obtained with DFO and Exjade (*SI Appendix, Fig. S8 A–D*). These results indicate that the E2F binding sites within the MYCN promoter play an important role in the response of neuroblastoma cells to iron chelation.

M606-Mediated MYCN Downregulation Occurs via E2F3. E2F is an activating transcription factor that binds to specific sites within the promoters of target genes. Studies have found that E2F1, E2F2, and E2F3 bind to the proximal MYCN promoter in MYCN-expressing neuroblastoma cell lines (16). More recently, E2F3 was found to be upregulated, alongside other transcription factors, in human and mouse neuroblastoma cells (26). Since the minimal region of the MYCN promoter necessary for the response to M606 contains the two inversely orientated and overlapping E2F sites, we investigated E2F binding to the MYCN promoter using chromatin immunoprecipitation (ChIP assays) in BE(2)-C cells. Both E2F1 and E2F3 were found to bind to MYCN at the transcriptional start site (TSS), but higher fold enrichment was observed with E2F3. Importantly, E2F3 binding was significantly reduced upon addition of M606 (Fig. 6A). We next examined whether E2F1 and E2F3 affected MYCN protein expression using transient siRNA knockdown in neuroblastoma cells. Depletion of E2F3 from BE(2)-C (Fig. 6B) and LAN-1 (*SI Appendix, Fig. S9*) cells decreased MYCN expression, whereas depletion of E2F1 had no effect. Furthermore, transient overexpression of E2F3, but not E2F1, rescued M606-mediated repression of the MYCN promoter (Fig. 6C). Moreover, overexpression of E2F3 resulted in increased MYCN promoter activity, but not when region 8 (containing the E2F3 binding site) was absent (*SI Appendix, Fig. S10*). These results further confirmed that M606-mediated downregulation of MYCN was via E2F3.

Since E2F3 is regulated by the retinoblastoma protein (RB), we investigated whether M606 affected RB phosphorylation, as

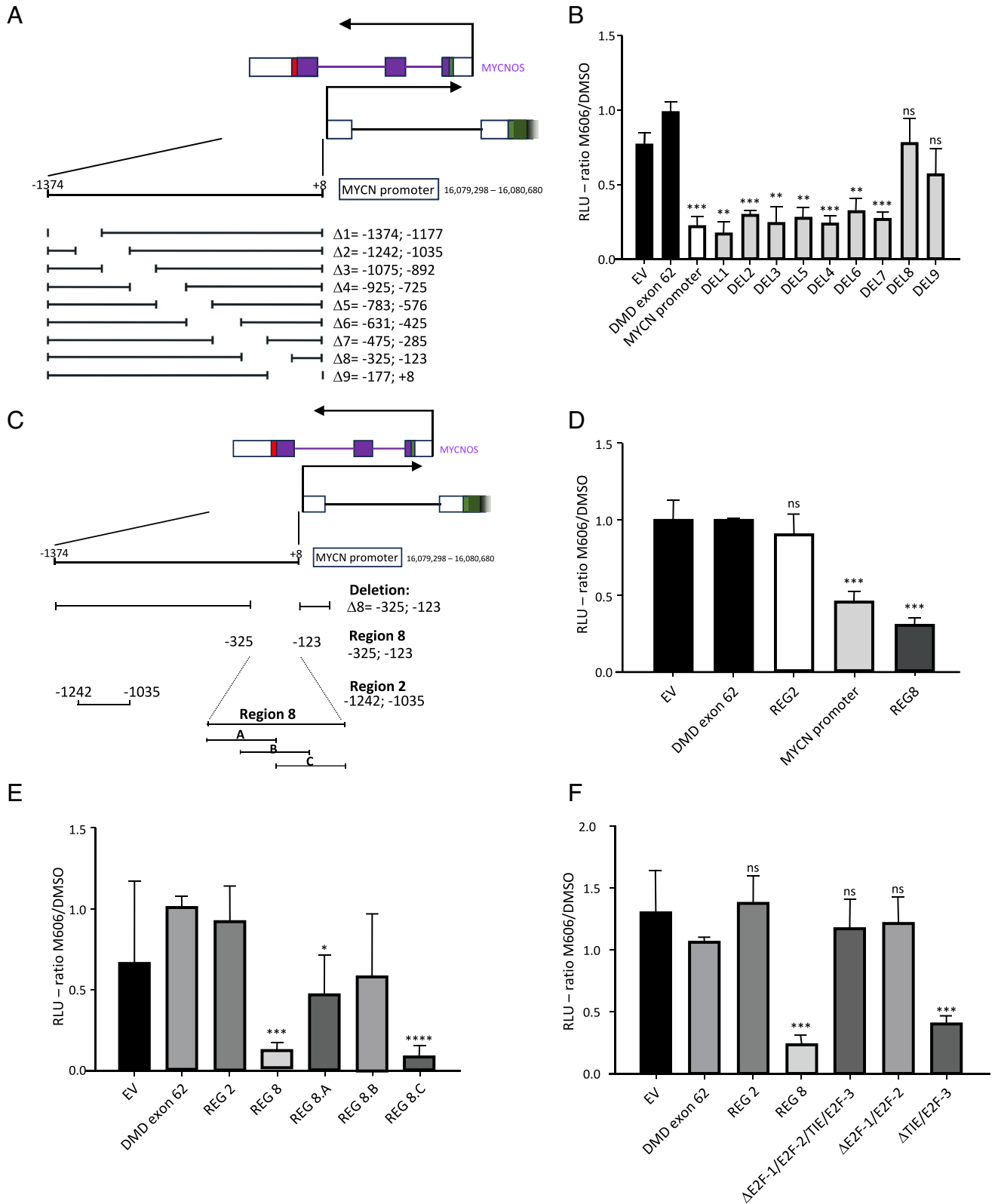


Fig. 5. Identification of the minimal region of the *MYCN* promoter required for the M606 response in BE(2)-C cells. (A) Graphical representation of pGL3_firefly luciferase-*MYCN* promoter deletion constructs. Distance from the transcription start site (black arrow) of *MYCN* is reported \pm N bp. (B) BE(2)-C cells were transfected with the indicated pGL3_firefly luciferase-*MYCN* promoter deletion constructs. After 6 h, the transfected cells were treated with 15 μ M M606 or DMSO vehicle control. *MYCN* promoter activity was analyzed 12 h posttreatment initiation. (C) Graphical representation showing further subdivision of Region 8 into three overlapping subregions. (D-F) Transfection of BE(2)-C with these subregion constructs and analysis of promoter activity. Data are presented as the mean normalized ratio of relative luciferase units (RLU) M606 treated to untreated \pm SD for three independent experiments. Statistically significant differences between each deletion mutant and the DMD Exon 62 construct were determined by the two-tailed unpaired *t* test using GraphPad software (**P* < 0.05; ***P* < 0.001; ****P* < 0.0001; *****P* < 0.00001).

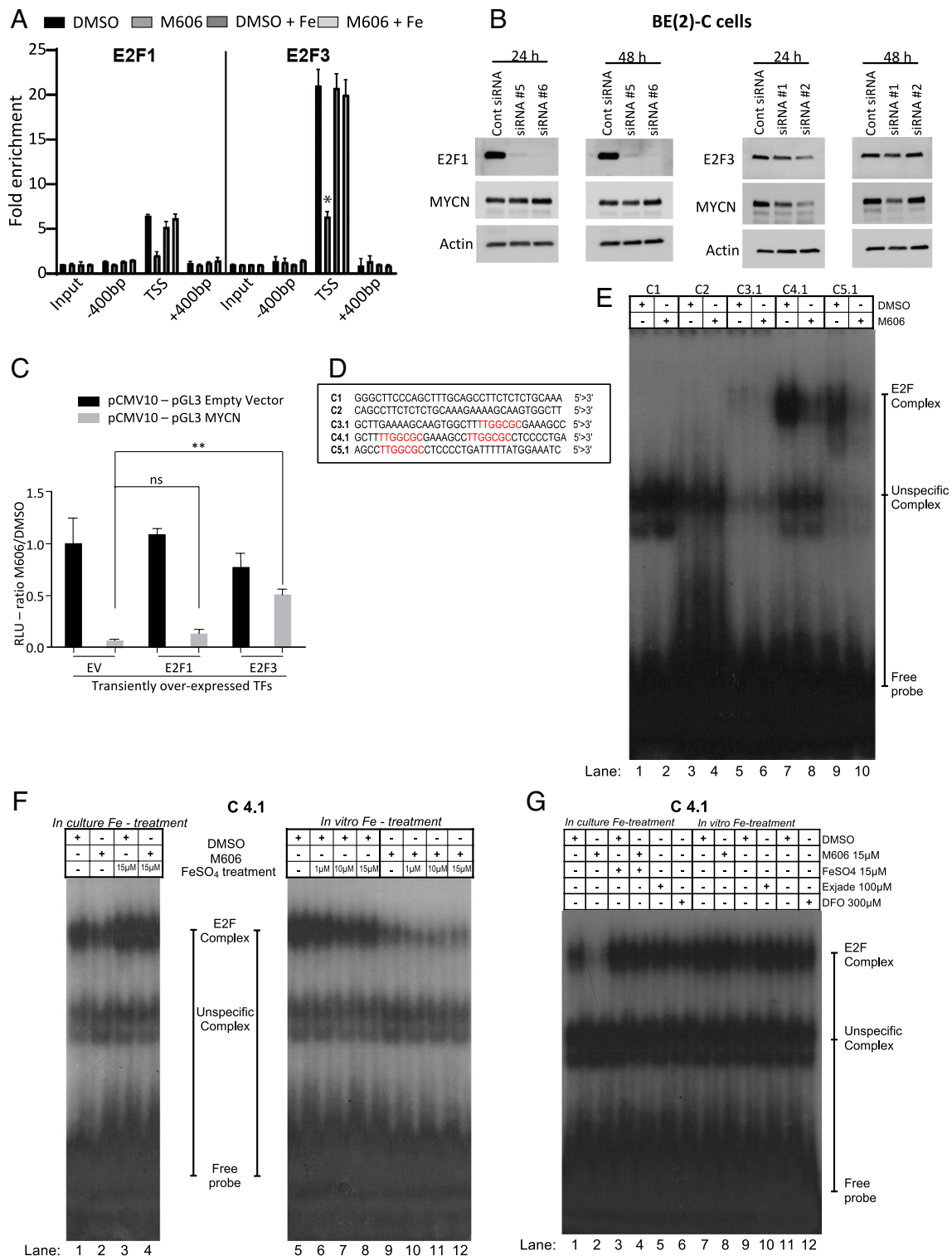


Fig. 6. M606-mediated downregulation of MYCN is mediated by E2F3 (A) ChIP analysis of E2F1 and E2F3 binding to the *MYCN* promoter in BE(2)-C cells following treatment with M606 (15 μM) for 12 h. (B) Western blot analysis of E2F1, E2F3, and MYCN following siRNA knockdown of E2F1 or E2F3 in BE(2)-C cells at 24 h and 48 h postinfection. (C) *MYCN* promoter activity using the luciferase assay was monitored in BE(2)-C cells following transient overexpression of E2F1 or E2F3. (D) Sequences of the probes used for EMSA. (E) EMSA was performed on nuclear extracts from BE(2)-C cell treated with DMSO or 15 μM M606 using the C3.1, C4.1, and C5.1 probes. (F) EMSA was performed using the C4.1 probe on nuclear extract from BE(2)-C cells treated with DMSO or 15 μM M606 in the presence or absence of increasing concentrations of iron (III) sulfate (Lanes 1–4). Nuclear extracts from BE(2)-C cells treated with M606 or DMSO were subsequently treated with iron (III) sulfate (Lanes 5–8), showing that iron can only mitigate the effects of M606 in intact cells. (G) EMSA comparing the response to C4.1 probe using nuclear extracts from BE(2)-C cells that were pretreated with DMSO (lanes 1, 3), M606 (lanes 2, 4), iron (III) sulfate (lanes 3, 4), Exjade (lane 5) or DFO (lane 6), and nuclear extracts from BE(2)-C cells to which DMSO (lanes 7, 9, 11), M606 (lane 8), Exjade (lane 10), or DFO (lane 12) were added to the in vitro binding reaction.

unphosphorylated RB can bind to E2F and block its ability to activate transcription. The main phosphorylation sites of RB involved in E2F binding are Thr821/826, Ser608/612, S788/S795, and T356/T373 (27, 28). As shown in *SI Appendix*,

Fig. S11, phosphorylation at Thr821/826, Ser608, and Ser795 were all reduced following treatment with M606, and to a lesser extent, DFO and Exjade. These effects were observed in as little as 6 h in BE(2)-C and LAN-1 cells, prior to seeing a major effect

on MYCN protein levels at 12 h. As expected, this reduction was reversed by the addition of excess iron. These data suggest that M606 activates RB by indirectly inhibiting its phosphorylation which in turn enables this tumor suppressor to bind to E2F proteins thereby repressing their ability to drive target gene transcription. However, although knockdown of RB did not affect E2F1 or E2F3 protein levels, it also did not reverse M606's inhibitory effects on MYCN expression (*SI Appendix, Fig. S12 A and B*). This suggests that other mechanisms in addition to RB phosphorylation are contributing to the action of M606 in downregulating MYCN.

To physically demonstrate that the E2F consensus site in the *MYCN* promoter is responsive to M606 treatment, electromobility gel shift assays (EMSA) were performed. The probes (Fig. 6D and *SI Appendix, Fig. S13*) were generated from Region 8C by further fragmenting this region into five subregions with the E2F consensus minimal region (TTGGCGC) present in only three of these (one in C3.1 and C5.1 and two in C4.1). When these probes were incubated with nuclear extracts obtained from BE(2)-C cells treated with DMSO for 12 h, we identified the formation of a specific E2F complex that formed only in the presence of an E2F consensus site (Fig. 6E, probes C3.1, C4.1, and C5.1 in lanes 5, 7, and 9, respectively). A stronger shift was observed with the C4.1 probe that contained both E2F sites. Moreover, M606 treatment reduced this specific shift (Fig. 6E, lanes 6, 8, and 10). To assess the specificity of the probes, competition assays were carried out using the E2F site from the *DHFR* promoter previously reported (29) to be bound mostly by E2F1 only, and the E2F binding site of the *CDC6* promoter, known to be bound mostly by E2F3 only (30). There was a clear reduction in the shift when a canonical and validated E2F3 probe was added in 5-fold excess to the reaction mix (*SI Appendix, Fig. S14A*, lanes 8 and 12); however, no reduction was observed in the presence of a 5-fold molar excess of the E2F1 probe (*SI Appendix, Fig. S14A*, lanes 7 and 11). Furthermore, we used a modified E2F1 probe mutated to reproduce an E2F3-specific consensus sequence and a modified E2F3 probe with the core region mutated to reproduce a typical E2F1 consensus sequence for additional competition studies. The cold-modified E2F1 probe could block the shift, whereas the modified E2F3 probe could not prevent the shift (*SI Appendix, Fig. S14B*). These experiments confirmed that the sequence in the *MYCN* promoter that was responsive to M606 had a greater binding affinity for E2F3 than E2F1.

The addition of excess iron (FeSO_4) in the culture medium prevented M606 from blocking the formation of the E2F complex (Fig. 6F, lanes 1–4). However, no changes in complex formation were observed when FeSO_4 was added directly to crude nuclear extracts from BE(2)-C cells treated with M606 (Fig. 6F, lane 9–12), demonstrating that iron recovery only acts when cells are growing in culture conditions. To compare M606 activity with other clinically available iron-chelating agents, particularly their ability to inhibit E2F binding to the *MYCN* promoter region, EMSA was performed with the C4.1 probe following treatment of BE(2)-C cells with M606 (15 μM), Exjade (100 μM), or DFO (300 μM) for 12 h prior to nuclear extraction. As expected, M606 reduced the specific shift compared to treatment with DMSO, and FeSO_4 abrogated this effect (Fig. 6G, Lanes 1–4), while no clear binding reduction was observed with Exjade or DFO (Fig. 6G, Lanes 5 and 6). There was also no effect following in vitro drug treatment of crude nuclear extracts (Fig. 6G lanes 7–12). Overall, these results demonstrate that M606 actively inhibits E2F3 protein binding to the minimal *MYCN* promoter, which can be reversed by the addition of FeSO_4 .

Discussion

Despite the aberrant activation of MYC family members in many types of cancers, the lack of FDA-approved MYC inhibitors highlights the difficulties in developing small molecule drugs for a widely considered “undruggable” target (31). Here, we have identified a small-molecule Myc inhibitor, M606, that downregulates MYCN and c-Myc proteins levels in Myc overexpressing tumor cell lines and delays tumor development in neuroblastoma-prone mice. Analysis of signaling pathways affected by M606 demonstrated inhibition of the Myc pathway and marked induction of the HIF1A pathway. Furthermore, M606 is a validated iron chelator that acts on the *MYCN* promoter via E2F3-mediated binding sites to reduce MYCN protein expression.

Although the crosstalk and interplay between MYC and HIF in cancer are complex and have been previously described [reviewed in (32)], our studies show that the effects of M606 on HIF1A and MYCN/c-Myc are independent of each other. HIF1A is preferentially expressed in both *MYCN*-amplified neuroblastoma cells and primary tumors compared to tissues without *MYCN* amplification (33). Under normoxic conditions or high cellular iron concentrations, the HIF1A protein is rapidly hydroxylated by iron-dependent prolyl hydroxylases (PHDs) for subsequent proteasomal degradation (34). However, the absence of iron inhibits the activity of PHDs due to their active sites having a requirement for iron (35). Analogs of M606 with an 8-hydroxyquinoline backbone are PHD inhibitors that stabilize HIF1A (36, 37), and this activity accounts for the observed induction of HIF1A following M606 treatment. Moreover, structural analogs of M606 without the capacity to chelate iron were not able to induce HIF1A or reduce MYCN, and lost the strong cytotoxic effect against neuroblastoma cell lines, indicating that the iron chelating properties of M606 are key to its cytotoxic effect.

Our metabolomic analyses showing that M606 exhibits strong effects on energy metabolism, and the finding that these effects can be rescued with the addition of iron, provide further evidence that the ability of M606 to bind cellular iron is key to its antiproliferative activity. Despite iron being an essential element required for normal cell proliferation and metabolism, altered iron metabolism has been implicated in tumor initiation and growth (38, 39). Although iron chelation therapy was originally designed to treat iron-overload disease, DFO became the first iron chelator used in cancer therapy, demonstrating antileukemic properties in a child with acute leukemia (40, 41). Moreover, high serum levels of the iron storage protein, ferritin, are prognostic of a poor outcome in children with neuroblastoma (42), suggesting that iron may play a role in promoting tumor cell growth. Subsequent investigation has shown that DFO treatment can cause marked cell death in neuroblastoma cell lines (43).

Other studies have shown that DFO treatment causes a marked decrease in *MYCN* mRNA expression and protein levels due to the inhibition of *MYCN* promoter activity and subsequent inhibition of transcription initiation (25). A Phase II trial of patients with neuroblastoma treated with a single course of DFO for 5 d combined with chemotherapy resulted in objective responses in 12 patients; however, patients also exhibited serious myelotoxic side effects (44). Further DFO clinical studies have shown variable responses in cancer patients attributable to several factors including the poor lipophilicity of the drug and short plasma half-life, leading to a search for new iron chelators for use in anticancer therapies (45, 46). Exjade is an orally bioavailable iron chelator with a better half-life than DFO and is commonly used to treat patients with iron-overload disease (47). Although it has shown

antitumor efficacy in preclinical models, a small clinical trial in hepatocellular carcinoma patients found dose-limiting toxicities in many patients and with no beneficial responses (48).

The finding that M606 has better cell penetration compared with DFO and Exjade with a strong effect on the *MYCN* promoter, enabled the identification of a 33 bp minimal response promoter region (C4.1) containing two E2F sites, which appear to be responsible for mediating its effect. The importance of these two E2F sites is supported by previous studies demonstrating the binding of the E2F1, E2F2, and E2F3 transcription factors to the *MYCN* promoter in neuroblastoma cell lines (16). E2F3 is up-regulated in *MYCN*-driven neural crest cell-derived neuroblastoma (26). More recently, E2F3 has been identified as a potential prognostic marker for Stage 4S neuroblastoma using in silico public neuroblastoma databases, with higher expression associated with impaired event-free survival (49). Our studies have shown a higher fold enrichment of E2F3 binding at the *MYCN* TSS compared to E2F1, consistent with the emerging role of E2F3 in neuroblastoma. Moreover, transient overexpression of E2F3, but not E2F1, overcame the M606-mediated repression of *MYCN* promoter activity.

Most genes regulated by E2F transcription factors have roles in controlling the cell cycle and their deregulation in cancer is associated with loss-of-function of the RB suppressor protein (50). Although RB silencing mutations are rare in neuroblastoma, high-level expression of cyclin D in association with kinases CDK4 and CDK6 effectively inactivate RB through hyperphosphorylation (51). Such phosphorylation dissociates RB from E2F factors allowing them to drive cell proliferation. CDK4/6 may be a primary target of M606, since it is known that iron chelation inhibits CDK activity, leading to RB becoming hypophosphorylated and allowing it to bind to E2F transcription factors and inhibit their activity (15). In addition, Myc and E2F have a combined role in controlling the cell cycle, and previous research has shown that RB deficiency leads specifically to Myc-dependent E2F3 accumulation and unrestrained cell proliferation (52). These findings are consistent with our results showing that E2F3 is critical for maintaining *MYCN* activity in neuroblastoma cells.

Neuroblastoma is a tumor with embryonal origins (53) and it is interesting to note that although functional redundancies exist between E2F1, E2F2, and E2F3, deletion of E2F3 alone results in embryonic lethality (54). E2F3 also has important roles in neurogenesis, neuronal survival, and mediating neuronal migration (55). Numerous studies have shown E2F3 overexpression in multiple cancers (54, 56), and high levels of this transcription factor are significantly associated with poor outcome in primary neuroblastoma (49, 57, 58). Overall, our results show that E2F3 is critical for maintaining *MYCN* activity in neuroblastoma cells. Recent studies have shown that targeting the RB-E2F pathway in high-risk neuroblastoma using CDK4/6 inhibitors holds significant promise (15, 59–61). M606, acting as an iron chelator, directly inhibits *MYCN* transcription via an E2F3-mediated response, and future studies combining this approach with CDK4/6 inhibition are warranted.

Materials and Methods

Cell Culture and Reagents. The following cell lines were used in this study: IMR-32, BE(2)-C, KELLY, LAN-1, NBL-WN, NBL-S, SY-5Y, and SH-EP (human neuroblastoma); HepG2 (hepatoblastoma); SAOS-2 (RB-mutated human osteosarcoma); MRC5 and HSF (nonmalignant human fibroblast cell lines). A description of the culture conditions employed in this study is included in *SI Appendix, Methods*.

Small Molecule Library Screening. We developed a cell-based readout system (SHR6-17) using SHEP neuroblastoma cells containing a MYC-responsive luciferase reporter that can respond to exogenously introduced *MYCN* (19). A

34,000 DIVERSet small molecule chemical library from ChemBridge Corporation was screened for molecules that inhibited the induction of the MYC-responsive reporter following the transduction of cells with *MYCN* lentivirus. Focused libraries were selected based on the structures of the most active hits and screened as described for the primary screen.

Western Blotting and Real-Time PCR. Western blotting was performed as described previously (*SI Appendix, Methods*). RNA was extracted using the RNeasy minikit (QIAGEN) and reverse transcribed with MMLV reverse transcriptase (Life Technologies) 48 h after knockdown. Gene expression was determined by qPCR using the ABI7900HT sequence detection system (Applied Biosystems, Thermo Fisher Scientific). The $\Delta\Delta C_t$ method was used to compare expression of target genes normalized to the expression of *GUSB*. TaqMan assays for *p27Kip1*, *thymidylate synthase*, *MYCN*, *erythropoietin*, and *VEGF-A* qPCR were purchased from ThermoFisher Scientific.

siRNA Knockdown. *MYCN* and *HIF1A* ON-TARGET plus SMARTPOOL siRNA was purchased from GE Dharmacon™. For studies looking at E2F1, E2F3, and RB, predesigned siRNAs were purchased from Qiagen. siRNA was transfected into cells using RNAiMAX according to the manufacturer's instructions.

EdU Incorporation Assays. EdU (5-ethynyl-2'-deoxyuridine) was added to SHR6-17 cells at a concentration of 10 μ g/ml for 1 h before fixation with 4% formaldehyde/PBS for 10 to 15 min at room temperature and washing three times with PBS. Cells were then permeabilized with 0.25% triton X-100 for 5 min and cell proliferation determined using the Click-iT EDU imaging kit with Alexa Fluor 488 azide assay according to the manufacturer's protocol (Thermo Fisher Scientific).

Colony Formation and Cytotoxicity Assays. Colony and cytotoxicity assays for the neuroblastoma cell lines were performed according to previously published methods (21, 62). For the colony assays, cells were plated at 500 cells/well in 6-well plates, treated with drugs for 72 h, and then incubated for 10 to 14 d. The colonies were stained and counted. For cytotoxic assays, cells were plated at 5,000 cells/well in 96-well plates and treated for 72 h before the addition of resazurin-based dye. Fluorescence was measured using the Victor luminometer from Perkin Elmer (CA).

Animal Experiments. All experimental animal procedures were approved by the University of New South Wales Animal Care and Ethics Committee according to the Animal Research Act, 1985 (NSW, Australia) and the Australian Code of Practice for Care and Use of Animals for Scientific Purposes (2013). The transgenic neuroblastoma mouse model overexpresses human *MYCN* in neuroectodermal cells and develops a murine equivalent of human neuroblastoma (20). Male and female mice were used in all experiments and maintained as previously described (20, 63). Tumor development was determined using abdominal palpation, which is routinely performed in our laboratory by experienced personnel (63) as described in *SI Appendix, Methods*.

Attagene Assay. The Attagene assay developed by Attagene Inc. (NC) is a homogeneous reporter system that quantitatively assesses the activity of multiple transcription factors (64). This system was used to determine the activity of multiple transcription factors in cells treated with M606. In this system, a library of reporter constructs (RTUs) was transfected into the reporter cells (HepG2). Each RTU contained a transcription factor-responsive promoter linked to a distinct downstream reporter sequence that was tagged with a unique endonuclease recognition site. Basal levels of transcription factor activity and levels after M606 treatment were determined following processing to produce distinct lengths of DNA fragments and quantitation by capillary electrophoresis.

¹³C Metabolic Labeling and Metabolomic Analyses. ¹³C-metabolic labeling and analysis protocols followed published methods (65, 66). BE(2)-C cells were plated at 5 × 10⁵/well in 6-well plates in DMEM/10% FBS. The cells were grown overnight before the medium was changed to MEM (Sigma-Aldrich #51416C) containing 10% FBS, NEAA, 2 g/L glucose, and 2 mM 50% ¹³C uniformly labeled glutamine. Alternately, for ¹³C glucose labeling, the same medium was used except that the glucose component was 50% ¹³C-uniformly labeled glucose (Sigma-Aldrich) and glutamine was unlabeled (2 mM), and a description of the methods employed in this study is included in *SI Appendix, Methods*.

Mass Spectrometry and LC-MS/MS Determination. Iron(III) chloride (97%) was from Sigma-Aldrich, and acetonitrile (190 grade) was from Ajax. Stock solutions (3.33 mM) of M606 and FeCl₃ were prepared in acetonitrile or water, respectively. A 1:3 Fe(III):M606 mixture was prepared, incubated at room temperature for 16 h, and analyzed by mass spectrometry, and a description of the methods employed in this study is included in *SI Appendix, Methods*.

The intracellular levels of M606, DFO, and Exjade were determined in BE(2)-C and LAN-1 cells using the Thermo Fisher TSQ Quantum LC-MS/MS system with a Phenomenex Kinetex 1.7u C18, 100A, 2.1 3 50 mm column. A description of the methods employed in this study is included in *SI Appendix, Methods*.

Luciferase Reporter Assay. Modulation of the activity of the full-length MYCN gene promoter and deletion mutants by M606 treatment (15 mM, 12 h) was analyzed using the dual-luciferase gene reporter assay. pGL3 construct carrying full MYCN gene promoter (pGL3-MYCN_{p_-1384}-2) was obtained by directional cloning using primers as listed in *SI Appendix, Table S1*. Serial deletion mutants were obtained by whole-around plasmid PCR amplification using pGL3-MYCN_{p_-1384}-2 as the starting plasmid DNA material. Luciferase reporter activity was measured using the Dual Luciferase Assay System (Promega). Data were normalized using DMD exon 62 as the control sample. Graphs were plotted as normalized ratios of M606 treated/untreated relative luciferase units (RLU). Data are presented as the mean of three independent experiments, error bars represent SD. Two-tailed, unpaired *t* tests were performed using GraphPad software (**P* < 0.05; ***P* < 0.01; ****P* < 0.005).

ChIP. For the endogenous E2F1 and E2F3 ChIP assays, 1 × 10⁷ cells were cross-linked using 1% formaldehyde, and the reaction was stopped using 0.125 M glycine. M606 treatments were performed as described for the luciferase assays and a description of the methods employed in this study is included in *SI Appendix, Methods*.

Electrophoretic Mobility Shift Assays (EMSA). The DNA probes used for EMSA and the cold competition assays were prepared from synthetic oligonucleotides. All the forward probes used in this study are shown in *SI Appendix, Fig. S13*. The DNA probe used as a wild-type (WT) cold competitor of the E2F1

binding region was the *DHFR* minimal gene promoter, prepared as previously described (29). The *CDC6* minimal gene promoter served as the WT cold competitor for the E2F3 binding region, prepared according to (30). The E2F1 and E2F3 probes were used to invert the core nucleotide of each E2F consensus (CC to GG in the E2F1 cold probe and GG to CC for the E2F3 cold probe), resulting in changes in the affinities of E2F1 and E2F3 in the cold competition assay. A description of the methods employed in this study is included in *SI Appendix, Methods*.

Data, Materials, and Software Availability. All study data are included in the article and/or *SI Appendix*.

ACKNOWLEDGMENTS. This study was supported by grants to M.H., G.M., and M.D.N. from the National Health and Medical Research Council (APP1016699, APP1132608), Cancer Institute NSW (10/TPG/1-03, 14/TPG/1-13), Tour de Cure, and Neuroblastoma Australia. This work was also supported by grants to G.P. from the Italian Association for Cancer Research (AIRC, grants IG15182 and IG24241) and by NIH SBIR grants (1R43CA110885-01 and 2R44CA110885-02A1) to C.A.B. and A.V.G. Children's Cancer Institute Australia is affiliated with University of New South Wales Sydney and the Sydney Children's Hospital Network. Portions of the paper were developed from the thesis of L.C.

Author affiliations: ^aChildren's Cancer Institute, Lowy Cancer Research Centre, University of New South Wales, Sydney, NSW 2031, Australia; ^bDepartment of Pharmacy and Biotechnology, University of Bologna, Bologna 40126, Italy; ^cBuffalo BioLabs, Limited Liability Company, Buffalo, NY 14203; ^dDepartment of Cell Stress Biology, Roswell Park Comprehensive Cancer Center, Buffalo, NY 14203; ^eGenome Protection, Inc., Buffalo, NY 14203; ^fAttagene Inc, NC 27560; ^gSchool of Medical Sciences, The University of Sydney, Sydney, NSW 2006, Australia; ^hKids Cancer Centre, Sydney Children's Hospital, Sydney, NSW 2031, Australia; ⁱSanford Burnham Prebys Medical Discovery Institute, La Jolla, CA 92037; ^jIstituto di Ricovero e Cura a Carattere Scientifico Azienda Ospedaliero-Universitaria di Bologna, Bologna 40126, Italy; and ^kUniversity of New South Wales Centre for Childhood Cancer Research, Sydney, NSW 2052, Australia

1. W. B. London *et al.*, Evidence for an age cutoff greater than 365 days for neuroblastoma risk group stratification in the children's oncology group. *J. Clin. Oncol.* **23**, 6459-6465 (2005).
2. K. K. Matthay *et al.*, Neuroblastoma. *Nat. Rev. Dis. Primers* **2**, 16078 (2016).
3. M. S. Irwin *et al.*, Revised neuroblastoma risk classification system: A report from the children's oncology group. *J. Clin. Oncol.* **39**, 3229-3241 (2021).
4. J. M. Maris, M. D. Hogarty, R. Bagatell, S. L. Cohn, Neuroblastoma. *Lancet* **369**, 2106-2120 (2007).
5. L. Moreno, L. V. Marshall, A. D. Pearson, At the frontier of progress for paediatric oncology: The neuroblastoma paradigm. *Br. Med. Bull.* **108**, 173-188 (2013).
6. B. Qiu, K. K. Matthay, Advancing therapy for neuroblastoma. *Nat. Rev. Clin. Oncol.* **19**, 515-533 (2022). 10.1038/s41571-022-00643-z.
7. G. M. Brodeur, R. C. Seeger, M. Schwab, H. E. Varmus, J. M. Bishop, Amplification of N-myc in untreated human neuroblastomas correlates with advanced disease stage. *Science* **224**, 1121-1124 (1984).
8. S. L. Cohn, D. A. Tweddle, MYCN amplification remains prognostically strong 20 years after its "clinical debut". *Eur. J. Cancer* **40**, 2639-2642 (2004).
9. N. Meyer, L. Z. Penn, Reflecting on 25 years with MYC. *Nat. Rev. Cancer* **8**, 976-990 (2008).
10. M. Vita, M. Henriksson, The Myc oncoprotein as a therapeutic target for human cancer. *Semin Cancer Biol.* **16**, 318-330 (2006).
11. E. V. Prochownik, P. K. Vogt, Therapeutic targeting of Myc. *Genes Cancer* **1**, 650-659 (2010).
12. S. K. Madden, A. D. de Araujo, M. Gerhardt, D. P. Fairlie, J. M. Mason, Taking the Myc out of cancer: Toward therapeutic strategies to directly inhibit c-Myc. *Mol. Cancer* **20**, 3 (2021).
13. C. J. Sherr, F. McCormick, The RB and p53 pathways in cancer. *Cancer Cell* **2**, 103-112 (2002).
14. L. Wang, H. Chen, C. Wang, Z. Hu, S. Yan, Negative regulator of E2F transcription factors links cell cycle checkpoint and DNA damage repair. *Proc. Natl. Acad. Sci. U. S. A.* **115**, E3837-E3845 (2018).
15. A. D'Otto *et al.*, KDM6B promotes activation of the oncogenic CDK4/6-pRB-E2F pathway by maintaining enhancer activity in MYCN-amplified neuroblastoma. *Nat. Commun.* **12**, 7204 (2021).
16. V. Strieder, W. Lutz, E2F proteins regulate MYCN expression in neuroblastomas. *J. Biol. Chem.* **278**, 2983-2989 (2003).
17. T. P. Wijesinghe, M. Dharmasivam, C. C. Dai, D. R. Richardson, Innovative therapies for neuroblastoma: The surprisingly potent role of iron chelation in up-regulating metastasis and tumor suppressors and down-regulating the key oncogene N-myc. *Pharmacol. Res.* **173**, 105889 (2021).
18. O. Ibrahim, J. O'Sullivan, Iron chelators in cancer therapy. *Biomaterials* **33**, 201-215 (2012).
19. C. A. Burkhardt, M. Haber, M. D. Norris, A. V. Gudkov, M. A. Nikiforov, "Cell-based methods for the identification of MYC-Inhibitory Small Molecules" in *The Myc Gene: Methods and Protocols*, L. Soucek, N. M. Sodik, Eds. (Humana Press, Totowa, NJ, 2013), pp. 255-264. 10.1007/978-1-62703-429-6_18.
20. W. A. Weiss, K. Aldape, G. Mohapatra, B. G. Feuerstein, J. M. Bishop, Targeted expression of MYCN causes neuroblastoma in transgenic mice. *EMBO J* **16**, 2985-2995 (1997).
21. L. D. Gamble *et al.*, Inhibition of polyamine synthesis and uptake reduces tumor progression and prolongs survival in mouse models of neuroblastoma. *Sci. Transl. Med.* **11**, eaau1099 (2019).
22. M. R. Doe, J. M. Ascano, M. Kaur, M. D. Cole, Myc posttranscriptionally induces HIF1 protein and target gene expression in normal and cancer cells. *Cancer Res.* **72**, 949-957 (2012).
23. J. W. Kim, I. Tchernyshyov, G. L. Semenza, C. V. Dang, HIF-1-mediated expression of pyruvate dehydrogenase kinase: A metabolic switch required for cellular adaptation to hypoxia. *Cell Metab.* **3**, 177-185 (2006).
24. L. Yu, X. Chen, X. Sun, L. Wang, S. Chen, The glycolytic switch in tumors: How many players are involved? *J. Cancer* **8**, 3430-3440 (2017).
25. L. Fan *et al.*, Inhibition of N-myc expression and induction of apoptosis by iron chelation in human neuroblastoma cells. *Cancer Res.* **61**, 1073-1079 (2001).
26. R. R. Olsen *et al.*, MYCN induces neuroblastoma in primary neural crest cells. *Oncogene* **36**, 5075-5082 (2017).
27. S. M. Rubin, A. L. Gall, N. Zheng, N. P. Pavletich, Structure of the Rb C-terminal domain bound to E2F1-DP1: A mechanism for phosphorylation-induced E2F release. *Cell* **123**, 1093-1106 (2005).
28. J. R. Burke, A. J. Deshong, J. G. Pelton, S. M. Rubin, Phosphorylation-induced conformational changes in the retinoblastoma protein inhibit E2F transactivation domain binding. *J. Biol. Chem.* **285**, 16286-16293 (2010).
29. M. A. Martinez-Balbás, U. M. Bauer, S. J. Nielsen, A. Brehm, T. Kouzarides, Regulation of E2F1 activity by acetylation. *EMBO J.* **19**, 662-671 (2000).
30. J. A. Freedman, J. T. Chang, L. Jakoi, J. R. Nevins, A combinatorial mechanism for determining the specificity of E2F activation and repression. *Oncogene* **28**, 2873-2881 (2009).
31. Z. Liu, S. S. Chen, S. Clarke, V. Veschi, C. J. Thiele, Targeting MYCN in pediatric and adult cancers. *Front. Oncol.* **10** (2021).
32. C. V. Dang, J.-W. Kim, P. Gao, J. Yuste, The interplay between MYC and HIF in cancer. *Nat. Rev. Cancer* **8**, 51-56 (2008).
33. G. Qing *et al.*, Combinatorial regulation of neuroblastoma tumor progression by N-Myc and hypoxia inducible factor HIF-1alpha. *Cancer Res.* **70**, 10351-10361 (2010).
34. C. Peyssonnaud, V. Nizet, R. S. Johnson, Role of the hypoxia inducible factors HIF in iron metabolism. *Cell Cycle* **7**, 28-32 (2008).
35. J. Myllyharju, Prolyl 4-hydroxylases, master regulators of the hypoxia response. *Acta Physiol. (Oxf)* **208**, 148-165 (2013).
36. N. C. Warshakoon *et al.*, Structure-based design, synthesis, and SAR evaluation of a new series of 8-hydroxyquinolines as HIF-1alpha prolyl hydroxylase inhibitors. *Bioorg. Med. Chem. Lett.* **16**, 5517-5522 (2006).
37. N. A. Smirnova *et al.*, Utilization of an in vivo reporter for high-throughput identification of branched small-molecule regulators of hypoxic adaptation. *Chem. Biol.* **17**, 380-391 (2010).
38. J. C. Kwok, D. R. Richardson, The iron metabolism of neoplastic cells: Alterations that facilitate proliferation? *Crit. Rev. Oncol. Hematol.* **42**, 65-78 (2002).
39. M. Jung, C. Mertens, E. Tomat, B. Brüne, Iron as a central player and promising target in cancer progression. *Int. J. Mol. Sci.* **20**, 273 (2019).
40. Z. Estrov *et al.*, In vitro and in vivo effects of deferoxamine in neonatal acute leukemia. *Blood* **69**, 757-761 (1987).
41. D. R. Richardson, Iron chelators as therapeutic agents for the treatment of cancer. *Crit. Rev. Oncol. Hematol.* **42**, 267-281 (2002).
42. H. W. Hann *et al.*, Prognostic importance of serum ferritin in patients with stages III and IV neuroblastoma: The children's cancer study group experience. *Cancer Res.* **45**, 2843-2848 (1985).

43. J. Blatt, S. Stitely, Antineuroblastoma activity of desferoxamine in human cell lines. *Cancer Res.* **47**, 1749 (1987).
44. A. Donfrancesco *et al.*, Deferoxamine, cyclophosphamide, etoposide, carboplatin, and thiotepa (D-CECaT): A new cytoreductive chelation-chemotherapy regimen in patients with advanced neuroblastoma. *Am. J. Clin. Oncol.* **15**, 319–322 (1992).
45. G. Abdelaal, S. Veuger, Reversing oncogenic transformation with iron chelation. *Oncotarget* **12**, 106–124 (2021).
46. J. L. Hamilton, J. N. Kizhakkedathu, Polymeric nanocarriers for the treatment of systemic iron overload. *Mol. Cell. Ther.* **3**, 3–3 (2015).
47. M. D. Cappellini, A. Taher, Deferasirox (Exjade) for the treatment of iron overload. *Acta Haematol.* **122**, 165–173 (2009).
48. I. Saeki *et al.*, Effects of an oral iron chelator, deferasirox, on advanced hepatocellular carcinoma. *World J. Gastroenterol.* **22**, 8967–8977 (2016).
49. S. Parodi, M. Ognibene, R. Haupt, A. Pezzolo, The over-expression of E2F3 might serve as prognostic marker for neuroblastoma patients with stage 4S disease. *Diagnostics (Basel)* **10**, 315 (2020).
50. I. Thurlings, A. de Bruin, E2F transcription factors control the roller coaster ride of cell cycle gene expression. *Methods Mol. Biol.* **1342**, 71–88 (2016).
51. J. J. Molenaar *et al.*, Cyclin D1 and CDK4 activity contribute to the undifferentiated phenotype in neuroblastoma. *Cancer Res.* **68**, 2599–2609 (2008).
52. H. Liu *et al.*, Redeployment of Myc and E2f1–3 drives Rb-deficient cell cycles. *Nat. Cell Biol.* **17**, 1036–1048 (2015).
53. G. M. Marshall *et al.*, The prenatal origins of cancer. *Nat. Rev. Cancer* **14**, 277–289 (2014).
54. I. Gamper *et al.*, Determination of the physiological and pathological roles of E2F3 in adult tissues. *Sci Rep.* **7**, 9932 (2017).
55. K. A. McClellan *et al.*, Unique requirement for Rb/E2F3 in neuronal migration: Evidence for cell cycle-independent functions. *Mol. Cell. Biol.* **27**, 4825–4843 (2007).
56. Y. Gao *et al.*, MiRNAs and E2F3: A complex network of reciprocal regulations in human cancers. *Oncotarget* **8**, 60624–60639 (2017).
57. M. Ognibene *et al.*, E2F3 gene expression is a potential negative prognostic marker for localized and MYCN not-amplified neuroblastoma: Results of in silico analysis of 786 samples. *Pediatr. Blood Cancer* **69**, e29800 (2022), 10.1002/pbc.29800, e29800.
58. H. Wang, X. Wang, L. Xu, J. Zhang, Prognostic analysis of E2F transcription factors E2F1 and E2F3 in four independent pediatric neuroblastoma cohorts. *BMC Pediatr.* **22**, 376 (2022).
59. B. Georger *et al.*, A phase I study of the CDK4/6 inhibitor ribociclib (LEE011) in pediatric patients with malignant rhabdoid tumors, neuroblastoma, and other solid tumors. *Clin. Cancer Res.* **23**, 2433–2441 (2017).
60. L. S. Hart *et al.*, Preclinical therapeutic synergy of MEK1/2 and CDK4/6 inhibition in neuroblastoma. *Clin. Cancer Res.* **23**, 1785–1796 (2017).
61. A. C. Wood *et al.*, Dual ALK and CDK4/6 inhibition demonstrates synergy against neuroblastoma. *Clin. Cancer Res.* **23**, 2856–2868 (2017).
62. L. Xiao *et al.*, Dual targeting of chromatin stability by the curaxin CBL0137 and histone deacetylase inhibitor panobinostat shows significant preclinical efficacy in neuroblastoma. *Clin. Cancer Res.* **27**, 4338–4352 (2021).
63. C. A. Burkhardt *et al.*, Effects of MYCN antisense oligonucleotide administration on tumorigenesis in a murine model of neuroblastoma. *J. Natl. Cancer Inst.* **95**, 1394–1403 (2003).
64. S. Romanov *et al.*, Homogeneous reporter system enables quantitative functional assessment of multiple transcription factors. *Nat. Methods.* **5**, 253–260 (2008).
65. B. Ratnikov *et al.*, Glutamate and asparagine cataplerosis underlie glutamine addiction in melanoma. *Oncotarget* **6**, 7379–7389 (2015).
66. D. A. Scott, Analysis of melanoma cell glutamine metabolism by stable isotope tracing and gas chromatography-mass spectrometry. *Methods Mol. Biol.* **2265**, 91–110 (2021).